Applied Catalysis B: Environmental 142–143 (2013) 668–676

Contents lists available at SciVerse ScienceDirect

Applied Catalysis B: Environmental

journal homepage: www.elsevier.com/locate/apcatb

Production of high carbon number hydrocarbon fuels from a lignin-derived α-O-4 phenolic dimer, benzyl phenyl ether, via isomerization of ether to alcohols on high-surface-area silica-alumina aerogel catalysts

Ji Sun Yoon[a,b], Yunsu Lee[a,b], Jihye Ryu[a,c], Young-A Kim[d], Eun Duck Park[d], Jae-Wook Choi[a], Jeong-Myeong Ha[a,e,f,*], Dong Jin Suh[a,e,f], Hyunjoo Lee[b]

[a] Clean Energy Research Center, Korea Institute of Science and Technology, Seoul 136-791, Republic of Korea
[b] Department of Chemical and Biomolecular Engineering, Yonsei University, Seoul 120-749, Republic of Korea
[c] Department of Chemical and Biological Engineering, Korea University, Seoul 136-701, Republic of Korea
[d] Division of Energy Systems Research and Department of Chemical Engineering, Ajou University, Suwon 443-749, Republic of Korea
[e] Department of Clean Energy and Chemical Engineering, University of Science and Technology, Daejeon 305-350, Republic of Korea
[f] Green School, Korea University, Seoul 136-701, Republic of Korea

ARTICLE INFO

Article history:
Received 13 December 2012
Received in revised form 30 April 2013
Accepted 21 May 2013
Available online 30 May 2013

Keywords:
Biomass
Lignin
Benzyl phenyl ether
Hydrodeoxygenation
Isomerization

ABSTRACT

Two-step hydrodeoxygenation of benzyl phenyl ether (BPE), a lignin-derived phenolic dimer containing an α-O-4 linkage, was performed to produce high carbon number saturated hydrocarbons. The ether linkage of BPE was first isomerized to alcohols of benzylphenols on the solid acid catalysts of silica (SA), alumina (AA), and silica-alumina aerogels (SAAs), which were further hydrodeoxygenated to saturated cyclic hydrocarbons on a silica-alumina-supported Ru catalyst. During the isomerization of BPE, noble-metal-free catalysts suppressed the formation of phenyl monomers but produced the phenolic dimers. SA, AA, and SAA-73 (Al/(Si + Al) = 0.73) exhibited negligible activity. However, SAA-38 and SAA-57 containing Al/(Si + Al) contents of 0.38 and 0.57, respectively, exhibited high catalytic activity among the prepared aerogel catalysts. The BPE conversion on SAA-38 reached 100% at a temperature range of 100-150 °C. The Brönsted acid sites appear to be catalytic active sites. On the basis of the predominant isomerization of phenyl ether to phenols over ether decomposition on the SAAs, the following second step of hydrodeoxygenation (HDO) after the first step of isomerization of BPE produced deoxygenated C13–19 cyclic hydrocarbons, as opposed to the saturated deoxygenated cyclic hydrocarbons produced trhough a one-step reaction process with silica-alumina-supported Ru catalysts, demonstrating this to be a promising process for producing high carbon number hydrocarbons from lignin dimers and oligomers.

1. Introduction

Fossil fuels have been used as energy sources and industrial feedstocks in all types of human activities. However, their expected declining supply and the effects of climate change have accelerated the development of alternative carbon-neutral resources [1,2]. Although different means of producing sustainable energy from wind, waves, geothermal heat, and solar energy have been developed, they cannot replace fossil fuels in carbon-based petrochemical industries. Biomass is a potential sustainable energy source and the only current alternative resource for the petroleum-based chemical industry because of its carbon-rich content [3–5]. For the past few decades, bioalcohols produced using an enzymatic fermentation of sugars combined with a thermochemical pretreatment have been widely investigated in the fields of molecular biology, biochemistry, and chemical engineering [6,7]. In these cellulose- and sugar-based processes and in the paper-manufacturing industry, lignin, a byproduct of the lignocellulose-to-bioalcohol and wood-to-paper processes, is considered a waste product. However, its rich carbon content and abundant aromatic monomers can be important resources for the carbon-based chemical industries [3–5,8,9].

Lignin is a natural amorphous polymer that consists of phenylpropane monomers, including *p*-hydroxylphenylpropane,

* Corresponding author at: Clean Energy Research Center, Korea Institute of Science and Technology, Seoul 136-791, Republic of Korea. Tel.: +82 2 958 5837; fax: +82 2 958 5209.
E-mail address: jmha@kist.re.kr (J.-M. Ha).

0926-3373/$ – see front matter © 2013 Published by Elsevier B.V.
http://dx.doi.org/10.1016/j.apcatb.2013.05.039

guaiacylpropane, and syringylpropane, which are covalently bonded to each other [8,10,11]. The depolymerization of lignin via thermochemical processes, such as pyrolysis [12,13], hydrothermal liquefaction [14–16], and catalytic decomposition [17–19], cleaves the ether and C—C linkages and leaves more processable fragments. The lignin fragments are then further converted to valuable fuels and chemicals. The catalytic treatment of depolymerized lignin or bio-oils may be an important step to produce valuable hydrocarbon fuels [20]. To upgrade the lignin fragments, the hydrodeoxygenation (HDO) of several monomeric and dimeric model compounds, such as guaiacol, eugenol, anisole, catechol, and phenol containing α-O-4 or β-O-4 ether linkages, have been studied [21,22]. Heterogeneous catalysts, such as zeolite-supported transition metals [23–26], molybdenum-based catalysts [27], solid acid-supported metals [28,29], and ionic-liquid assisted metals [30], along with homogeneous catalysts [31] were used for the HDO of phenolic compounds. The catalytic reaction network has also been studied [27,29,32,33].

While most HDO processes are accompanied by the catalytic cracking of lignin oligomers to monomers [22], we suggested the catalytic HDO of lignin fragments to a deoxygenated high carbon number dimer without cracking. This process was elucidated using a probable lignin model compound, benzyl phenyl ether containing an α-O-4 linkage, in this study. The reaction route to the high carbon number hydrocarbons suppressing the cleavage of ether linkages may be useful to selectively produce diesel and jet fuels containing high carbon number hydrocarbons. Benzyl phenyl ether was selected as a model reactant for lignin or lignin-derived oligomers because the existence of the α-O-4 linkage in lignin has been reported along with the mainly observed β-O-4 linkage [11]. Additionally, the HDO of phenolic dimers with an α-O-4 linkage has been studied [23,34–36]. In this study, benzyl phenyl ether was first isomerized to alcohols and then further hydrodeoxygenated to saturated deoxygenated hydrocarbons, which produced the higher carbon number hydrocarbons compared to that by the direct hydrodeoxygenation. We demonstrated that this two-step catalytic conversion of benzyl phenyl ether on solid acid and bifunctional catalysts produced high carbon number hydrocarbon fuels without ether cleavage. The catalytic isomerization of benzyl phenyl ether (BPE) to benzylphenols was studied and the active sites for the isomerization on the aerogel catalysts were investigated using solid characterization methods, including temperature-programmed desorption (TPD), Fourier-transformed infrared (FT-IR), and nuclear magnetic resonance (NMR). This study demonstrates that the proposed process will be useful for converting lignin fragments to high carbon number hydrocarbon fuels, including diesel and jet fuels.

2. Experimental

2.1. Materials

All chemicals were used without further purification unless otherwise mentioned. Tetraethyl-*ortho*-silicate (TEOS, 98%), propylene oxide (PO, 99%), benzyl phenyl ether (BPE, 98%), *n*-decane (99%), phenol (99%), 2-benzylphenol (2BP, 98%), 4-benzylphenol (4BP, 99%), toluene (anhydrous, 99.8%), benzene (anhydrous, 99.8%), cyclohexanone (99.8%), and methylcyclohexane (anhydrous, 99%), 2,6-di-*tert*-butylpyridine (2,6-DTBP, 97%), ruthenium (III) chloride hydrate ($RuCl_3{\cdot}xH_2O$, 49% Ru), and commercial silica-alumina powder (CSA, grade 135) were purchased from Aldrich (Milwaukee, Wisconsin, USA). Methanol (extra pure grade, 99.5%) was purchased from Daejung (Seoul, Korea). Aluminum (III) chloride hexahydrate ($AlCl_3{\cdot}6H_2O$, 97%), aqueous ammonia (NH_3 (*aq.*), >28 wt%), and ammonium fluoride (NH_4F, 97%) were purchased from Junsei (Tokyo, Japan). Nitric acid (HNO_3, 61%) and cyclohexane (99.5%) were purchased from Yakuri (Kyoto, Japan). DI water (18.2 MΩ cm) was prepared using an aqua MAX-Ultra 370 Series water purification system (Young Lin Instrument, Anyang, Korea). Helium (He, 99.999%), hydrogen (H_2, 99.999%), oxygen (O_2, 5%, v/v) in helium, and ammonia (NH_3, 5%, v/v) in helium were purchased from Shinyang Sanso (Seoul, Korea).

2.2. Preparation of catalysts

2.2.1. Preparation of the silica-alumina, alumina, and silica aerogels

The silica-alumina gel was prepared using the reactants listed in Table 1. TEOS was added to $AlCl_3$ dissolved in methanol while stirring. The mixture was further stirred for 10 min. Dilute aqueous nitric acid solution was then added to the mixture and stirred for 30 min. DI water was added to the solution under vigorous stirring and further stirred for 1 h. PO was added to the mixture 2 or 3 times in 5-min-intervals. The gelation time to form the wet gel (or alcogel) was determined based on the disappearance of the vortex. The alumina gel was prepared using the reactants listed in Table 1. A mixture of aluminum chloride, ethanol, and aqueous nitric acid was stirred for 30 min to produce a homogeneous solution. DI water was added to the solution while stirring. After 90 min, PO was added to the mixture. The silica gel was prepared using a method described in the literature (Table 1) [37,38]. After aging for 2–4 days, the alcogel containing alcohol entrapped in the gel network was dried using a supercritical drying process with CO_2 in a supercritical extraction system at 70 °C and 13 MPa. The silica and silica-alumina aerogels were calcined at 600 °C for 6 h under static air. The alumina aerogel was calcined at 500 °C for 4 h under flowing air. The prepared aerogel powders were ground and sieved (<75 μm).

2.2.2. Preparation of the silica-alumina supported Ru catalyst

Ru was impregnated onto commercial silica-alumina (CSA) and SAA-38 using an incipient-wetness method. After drying for 16 h at 105 °C in an oven, the catalyst was reduced under an H_2 flow at 350 °C for 2 h (2.02 wt% Ru/CSA). The prepared catalyst powder was ground and sieved (<75 μm).

2.3. Characterizations

The compositions of the prepared catalysts were measured using inductively coupled plasma atomic emission spectroscopy (ICP-AES; Polyscan-61E, Thermo Electron Corp., Winsford, Cheshire, UK). The silica-alumina aerogels containing Al/(Si + Al) = 0.38, 0.57, and 0.73 (mol/mol), based on the ICP-AES results, were denoted as SAA-38, SAA-57, and SAA-73, respectively. The silica aerogel and alumina aerogel were denoted as SA and AA, respectively. N_2-physisorption was performed using an ASAP 2010 and ASAP 2020 (Micromeritics, Norcross, GA, USA) to measure the pore volume, the Brunauer–Emmett–Teller (BET) surface area, and the Barrett–Joyner–Halenda (BJH) model pore size distribution [39–41]. NH_3-temperature programmed desorption (NH_3-TPD) was performed using a BELCAT-B temperature programming unit (BELCAT, Osaka, Japan) equipped with a thermal conductivity detector (TCD), as described in the literature [29]. The FT-IR spectra of the catalysts adsorbing pyridine (pyridine-FT-IR) were obtained using a Nicolet 6700 FT-IR spectrometer (Thermo Scientific, West Palm Beach, FL, USA) equipped with a MCT-A detector averaging 64 scans over a range of 1400–1700 cm^{-1} with a resolution of 4 cm^{-1}. The wavenumber range used in this study was selected to observe the ring vibrations of adsorbed pyridine. A self-pelletized catalyst (0.02 g) was installed in an IR cell with a CaF_2 window and degassed at 300 °C to remove physisorbed moisture on the catalyst through a Schlenk line connecting to the IR cell.

Table 1
Preparation conditions for the silica, alumina, and silica-alumina aerogels.

	SA	SAA-38	SAA-57	SAA-73	AA
Si:Al (mol:mol)	1:0	2:1	1:1	1:2	0:1
TEOS (mL)	21.41	21.41	21.41	21.41	0
$AlCl_3{\cdot}6H_2O$ (g)	–	12.44	24.88	49.76	14.93
Methanol (mL)	61.0	61.0	61.0	61.0	0
Ethanol (mL)	0	0	0	0	123.7
Nitric acid (mL, *aq.*, 61 wt%)	0	0.187	0.187	0.187	0.44
Ammonia (mL, *aq.*, 28 wt%)	0.069	0	0	0	0
Ammonium fluoride (mL)	0.004	0	0	0	0
PO (mL)	0	14.14	28.27	56.55	12.72
DI water (mL)	7.227	7.227	7.227	7.227	3.24

Prior to the pyridine adsorption process, the baseline was recorded using the degassed catalyst pellet. The excess vaporized pyridine was adsorbed onto the catalyst surface at room temperature for 30 min, and the catalyst pellet was evacuated at 100 °C for 90 min then cooled to room temperature, at which the FT-IR spectra were obtained. The catalyst pellet was further evacuated at 250 °C for 90 min then cooled to room temperature at which the FT-IR spectra were obtained again. The Brönsted acid (BA) and Lewis acid (LA) sites were counted using the peaks at 1548 cm^{-1} (BA) and 1446 cm^{-1} (LA), respectively, and their extinction coefficients [42]:

$$\text{BA sites(mmol/g-catalyst)} = 1.88 \times IA_{BA} \times \frac{R^2}{W}$$

$$\text{LA sites(mmol/g-catalyst)} = 1.42 \times IA_{LA} \times \frac{R^2}{W}$$

where IA_{BA} is the integrated absorbance of the BA band at 1548 cm^{-1}, IA_{LA} is the integrated absorbance of the LA band at 1446 cm^{-1}, R is the radius of the catalyst pellet (0.65 cm), and W is the weight of the pellet (mg). Magic-angle spinning (MAS) ^{27}Al NMR spectra were recorded at a frequency of 15 MHz on a Varian 400 NMR spectrometer equipped with a 9.4 T magnet. The spectra were recorded using a 2 μs excitation pulse, a 1 s relaxation delay, a 3.2 ms acquisition time, and a 4 μs contact time with 1000 repetition times. ^{29}Si MAS NMR spectra were obtained at a frequency of 5 MHz on a Varian 200 NMR spectrometer equipped with a 4.7 T magnet. The spectra were recorded using a 4 μs excitation pulse, a 1 s relaxation delay, a 50 ms acquisition time, and a 4 μs contact time with 1000 repetitions.

2.4. Catalysis

The catalytic isomerization of benzyl phenyl ether (BPE) was performed in a 160-mL Hastelloy C®-276 batch reactor which was filled with the catalyst (0.1 g or 0.01 g) and 0.05 M BPE solution (40 mL) dissolved in *n*-decane. The reactor was filled with 5 bar He, and 5, 10, 20, 30, or 40 bar H_2 at room temperature. Each isothermal reaction was performed at room temperature, 70, 100, 150, 200, and 250 °C for 1 h. The reaction was also performed under 5 bar He for 100 h. When a reaction was complete, the reactor was cooled to room temperature using cooling water. The activity of the catalysts was further studied by adding 2,6-di-*tert*-butylpyridine (2,6-DTBP; 0.18, 0.45, 0.89, 2.50, and 26.7 μmol) to the reactant BPE solution, which was expected to block the Brönsted acid sites on the catalysts, to confirm the effects of acidity. In addition to isomerization, the catalytic hydrodeoxygenation (HDO) of BPE was performed using three different procedures: (i) a one-step process of directly hydrodeoxygenated BPE at 250 °C under 40 bar H_2 using 2.02 wt% Ru/CSA (0.1 g), (ii) a two-step process of isomerizing BPE at 100 °C under 5 bar H_2 using SAA-38 (0.1 g) followed by HDO using 2.02 wt% Ru/CSA (0.1 g) at 250 °C under 40 bar H_2, and (iii) a one-step process of BPE HDO at 250 °C under 40 bar H_2 using 2.02 wt% Ru/CSA (0.1 g) and SAA-38 (0.1 g). For all catalytic reactions, the liquid-phase products were analyzed by a GC (Younglin, Acme 6000E), equipped with a flame ionization detector (FID), using an HP-5 capillary column (60 m × 0.25 mm × 0.25 μm). The products were identified with a GC–MS (Agilent Technologies, 7890A, HP-5 capillary column, 60 m × 0.25 mm × 0.25 μm). The conversion, selectivity, and yield of the reactions and material balance were determined with the yield sum based on the moles of carbon atoms using the following equations:

$$\text{Conversion}(\%) = \frac{C_0 - C_e}{C_0} \times 100,$$

$$\text{Selectivity}(\%) = \frac{C_i}{C_0 - C_e} \times \frac{M_i}{M_0} \times 100,$$

$$\text{Yield}(\%) = \frac{C_i}{C_0} \times \frac{M_i}{M_0} \times 100,$$

where C_0 is the initial concentration of BPE before a reaction, C_e is the existing concentration of BPE after a reaction, C_i is the concentration of an identified product, M_0 is the moles of carbon atoms which BPE contains, and M_i is the moles of carbon atoms which the product contains.

3. Results and discussion

3.1. Conversion of benzyl phenyl ether to benzylphenols on precious-metal-free aerogel catalysts

In order to avoid ether cleavage during the HDO process, the isomerization of aryl ether to phenols was performed. Benzyl phenyl ether (BPE), the lignin-derived phenolic dimer selected for use in this study, was converted to 2-benzylphenol (2BP), 4-benzylphenol (4BP), phenol, and other minor products on the prepared aerogel catalysts (Fig. 1). The two major products of 2BP and 4BP were obtained by the intramolecular rearrangement, and the third product of phenol was obtained via the undesirable outcome of ether cleavage. The formation of toluene, the counterpart of phenol on the ether cleavage, was negligible (below 0.1% yield) in all the observed instances, which may be related to the formation of trimers, including dibenzylphenols. While the formation of dibenzylphenols was observed on SAA-38 and SAA-57, exhibiting compositions of 24 and 13 area%, respectively, based on the GC-FID result [43], the missing toluene may contribute to the formation of dibenzyl phenols because each dibenzyl phenol molecule may form from one benzyl phenol and one toluene, that is, one phenol and two toluenes.

The conversion of BPE and the selectivity to 2BP were the highest with SAA-38, but the BPE conversion was very low or negligible with SA, SAA-73, and AA. BPE conversion on SAA-38 reached 93% at 100 °C and 100% at 150 °C and higher, but selectivity to 2BP decreased from 62% at 100 °C to 38% at 250 °C. When observing the effects of the H_2 or He environments, H_2 did not seem to affect the

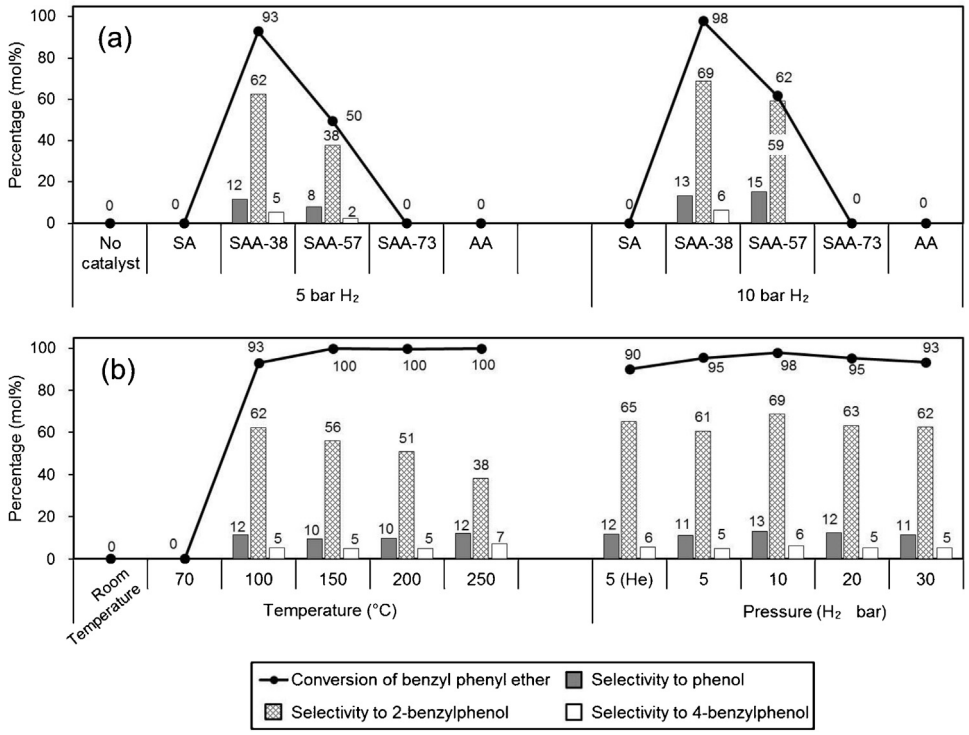

Fig. 1. Catalysis results on the aerogel catalysts. (a) Catalytic performance of the catalysts at 100 °C under 5 bar H_2 (left) and 10 bar H_2 (right). (b) Catalytic performance of SAA-38 with respect to reaction temperature at 5 bar H_2 (left) and H_2 pressure at 100 °C (right). (0.05 M BPE dissolved in 40 mL *n*-decane were converted using 0.1 g catalyst.) All the catalysis results were obtained after 1 h batch reactions.

conversion of BPE significantly. We continued using a sufficient H_2 environment in this study because of the possible H_2-consuming ether bond cleavage, despite the fact that H_2 is poorly adsorbed on a solid acid catalyst surface. Unlike previously observed HDO processes on acid-supported precious metal catalysts [29], a significant decrease in the H_2 pressure was not observed during the reaction, indicating negligible consumption of H_2.

The catalyst was allowed to be deactivated by the long-term reaction of BPE on SAA-38 (0.01 g in Table 2 compared with 0.1 g in Fig. 1) at 100 °C and 5 bar He. There was no H_2 supply so as to ensure a poor H_2 environment during the reaction. The BPE conversion increased from 17.9 (after 1 h) to 43.5% (after 100 h) and the 2BP selectivity increased from 38.4 (after 1 h) to 80.6% (after 100 h). The selectivities to the two other major products of 4BP and phenol did not significantly change upon a longer reaction time. These observations indicate that (i) deactivation of the solid acid catalysts may not be significant for the conversion of BPE, and (ii) there may be a reaction pathway that predominantly produces 2BP on the solid acid aerogel catalysts. During the 100-h reaction, the molar ratio of (2BP)/(4BP) increased from 9.8 to 17.5 because of the possibly higher stability of 2BP or the possible isomerization of 4BP to 2BP. The higher stability or the preferred formation of 2BP to 4BP was confirmed when the catalysis of an equimolar mixture of 2BP and 4BP was performed on SAA-38 at 100 °C for 24 h, exhibiting an increased molar ratio of (2BP)/(4BP) from 1 to 1.3.

Based on the reaction pathways reported in the literature [35,44–56], we attempted to confirm the routes of BPE to 2BP, 4BP, phenol, and other products using carefully designed control experiments (Fig. 1 and Table 2). The predominant formation of 2BP over 4BP is attributable to the intramolecular rearrangement such as the Claisen rearrangement [57,58], which first fills the *ortho*-position followed by an allylic group's migration to the *para*-position via *para*-Claisen rearrangement without filling the *meta*-position. Claisen rearrangement has been introduced to explain radical reactions by thermal decomposition at high temperatures (300–500 °C) [44–46,52,59], while also being used to explain catalytic isomerization at low temperatures (25–110 °C) [43,58,60–62] which is similar to the temperature range used in this study. The preferred formation of 2BP was further studied by observing the product selectivity of (2BP)/(4BP) while changing the reaction temperature, H_2 pressure, Al/(Si + Al) ratio, and reaction time (Fig. 1). The ratio of (2BP)/(4BP), or the formation of 2BP, decreased with an increase the reaction temperature from 100 to 250 °C. In addition, the (2BP)/(4BP) ratio was nearly constant with different H_2 pressures, indicating the negligible dependence of the catalytic activity on the pressure. The effect of Al/(Si + Al) on the selectivity of 2BP over 4BP was not clear because an appreciable conversion of BPE was observed only with SAA-38 and SAA-57. These observations of catalytic activities are further discussed in the following sections using the characterization results of the aerogel catalysts.

3.2. Characterizations of the catalysts

3.2.1. N_2-physisorption

The nanoscopic structures of the aerogel catalysts were observed using N_2-physisorption, which confirmed their mesoporosity, large pore volume, and high surface area, as expected from a review of the literature (Table 3 and Fig. S1) [37,38,40,41,63]. All the aerogel catalysts exhibited monodisperse mesopores (approximately 5–50 nm) with high BET surface areas of 244–963 $m^2\ g^{-1}$. The SAAs exhibited sharper pore size distributions with smaller pore diameters and pore volumes, while SA and AA had broader pore size distributions with larger pore diameters and pore volumes. Although the highly active SAA-38 and SAA-57 exhibited large surface areas of 467–481 $m^2\ g^{-1}$, the inactive or less active SA, SAA-73, and AA did not exhibit significantly smaller surface areas; thus, this parameter does not explain the stark difference in their catalytic activities.

Table 2
Catalysis results with respect to reaction time at 100 °C under 5 bar He using SAA-38 (0.01 g catalyst, 0.05 M BPE in 40 mL *n*-decane).

	Conversion (mol%)	Selectivity (mol%)			Yield of (Phenol + 2BP + 4BP) (mol%)
		Phenol	2BP	4BP	
5 bar He, 1 h	17.9	13.3	38.4	3.9	9.9
5 bar He, 100 h	43.5	11.5	80.6	4.6	42.0

Table 3
Pore structures of the aerogel catalysts.

	S_{BET}[a] ($m^2\ g^{-1}$)	S_{micro}[b] ($m^2\ g^{-1}$)	$S_{external}$[c] ($m^2\ g^{-1}$)	V_{pore}[d] ($cm^3\ g^{-1}$)	D_{pore}[e] (nm)
SA	963	76	887	3.8	27
SAA-38	467	32	435	1.2	10
SAA-57	481	48	433	1.7	12
SAA-73	244	33	211	1.0	14
AA	392	38	354	2.8	18

[a] BET surface area.
[b] Micropore area obtained by *t*-plot analysis.
[c] External surface area obtained by *t*-plot analysis combined with the BET surface area.
[d] Single point adsorption total pore volume.
[e] Desorption pore diameter peak obtained by the BJH method.

3.2.2. NH_3-TPD

Predicting the catalytic activity depending on the acidity on the basis of studies indicating that BPE isomerization occurs on acid catalysts [61,64], the acidity of the catalysts was measured using NH_3-TPD (Fig. 2 and Table 4). High temperature acid sites (350–850 °C, HR), as measured by NH_3 desorbed at 350–850 °C, are generally important in catalysis [65,66]. SAA-38, the most active catalyst in this study, exhibited the lowest number of total acid sites (TR) or HR, indicating that the catalytic activity did not directly depend on the number of total acid sites. When the low temperature (100–350 °C, LR) and high temperature acid sites (350–850 °C, HR) were compared, the more catalytic activity was observed with the fewer HR. The amount of LR was not significantly different except for SA which exhibited a negligible amount of LR.. The total number of acid sites measured using NH_3 desorbed at 100–850 °C (TR) increased with increasing Al/(Si + Al) in the following order: AA > SAA-73 > SAA-57 > SAA-38 > SA. The amount of HR increased with an increase in Al/(Si + Al) except SA in the following order: SAA-38 > SAA-57 > SAA-73 > AA. SAA-38 and SAA-57, containing fewer acid sites, exhibited high BPE conversions. However, SA, SAA-73, and AA, containing more acid sites, exhibited negligible BPE conversions (Figs. 1 and S3). These observations indicate that the number of TR or HR does not determine the catalytic activity, but the increasing ratio of LR to TR or LR to HR more significantly affects the catalytic activity. Identifying TPD peaks remains controversial, although there have been attempts to identify LR and HR in NH-TPD for zeolites [66–70] and amorphous silica-alumina [65,71]; thus, our remark on the importance of LR/TR cannot be easily justified. Instead, the type of acid may play an important role in catalysis process, which requires further investigation of the types of acids as part of the efforts to understand BPE isomerization.

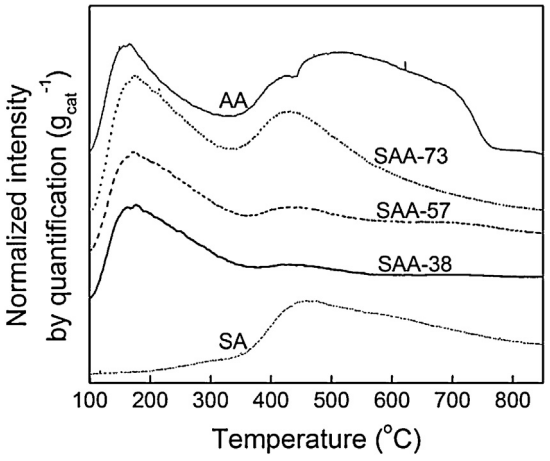

Fig. 2. NH_3-TPD results of the catalysts.

3.2.3. Pyridine-FT-IR

Because the numbers of acid sites could not explain the BPE isomerization activity, the types of catalysts were further analyzed using pyridine-FT-IR, which identifies Lewis (LAs) or Brönsted acids (BA) (Table 4, Figs. S2 and S3) [72,73]. The distinct bands of BAs were observed at 1637–1640 and 1548 cm^{-1} in all catalysts except for SA. The peaks at 1446 and 1594–1598 cm^{-1} appeared to represent the interaction via hydrogen bonds, which virtually disappeared when evacuated at 250 °C. The distinct bands of LAs were identified at 1622–1623, 1614–1616, 1578, and 1450–1454 cm^{-1} in all the catalysts. The absorption at 1492 cm^{-1} was observed in all catalysts except SA, which represents a mixture of hydrogen bond, BA, and LA. SA did not exhibit absorption bands at 1548 (BA) and 1492 cm^{-1} (BA and LA), indicating that SA did not contain BA. The ratio of BA/LA was calculated using the absorption bands at 1548 (BA) and 1450 cm^{-1} (LA) [42] observing that the BA/LA ration was larger on the more active SAA-38 and SAA-57 but smaller on the inactive SAA-73, AA, and SA. These observations indicate that the BPE isomerization activity was improved by BA, but that it was possibly inhibited by LA.

3.2.4. ^{27}Al- and ^{29}Si-NMR

The acidity of the catalyst surface, as previously discussed after analyzing the NH_3-TPD and pyridine-FT-IR results,, was further examined in observations of the solid structures by magic-angle spinning (MAS) ^{29}Si-and ^{27}Al-NMR. The ^{29}Si NMR results exhibited strong chemical shift peaks at −108.7 ppm (Q^4), −101.1 ppm (Q^3) and −91.1 (Q^2) for SA [74]. However, broad peaks for the SAAs were attributed to Si surrounded by Al atoms, in this case Q^4(1Al) (−98.8 ppm) for SAA-38, Q^4(2Al) (−93.8 ppm) for SAA-57, and Q^4(3Al) (−87.9 ppm) in SAA-73 (Fig. 4 (a)) [74]. Q^n represents the tetrahedral symmetry of SiO_2 with *n* denoting the number of Si—O—Si connections in SA, and mAl represents the number (m) of Al species bound to the Q^n unit. The ^{27}Al NMR results exhibited two distinct peaks at 44 ppm (tetrahedral symmetry, Al(IV)) and close to −4.8 ppm (octahedral symmetry, Al(VI)) (Fig. 3(b)) [74]. The ratio

Table 4
Concentrations of the acid sites measured by NH_3-TPD and pyridine-FT-IR.

Catalyst	The amount of acidic sites (mmol/g-catalyst)											
	NH_3-TPD				Pyridine-FT-IR							
	LR	HR	TR	LR/TR	Evacuated at 100 °C				Evacuated at 250 °C			
					BA	LA	TA	BA/LA	BA	LA	TA	BA/LA
SA	0.03	0.73	0.76	0.04	0.00	0.25	0.25	0.00	0.00	0.04	0.04	0.00
SAA-38	0.65	0.28	0.93	0.70	0.13	0.26	0.39	0.51	0.13	0.12	0.25	1.07
SAA-57	0.77	0.46	1.23	0.63	0.12	0.36	0.48	0.35	0.11	0.17	0.28	0.67
SAA-73	1.07	1.03	2.10	0.51	0.06	0.42	0.48	0.15	0.06	0.17	0.24	0.37
AA	0.68	1.44	2.12	0.32	0.01[a]	0.08[a]	0.08[a]	0.11	0.00[a]	0.06[a]	0.06[a]	0.02

[a] The pelletized AA was cracked slightly during pretreatment at 300 °C producing low values of BA and LA.

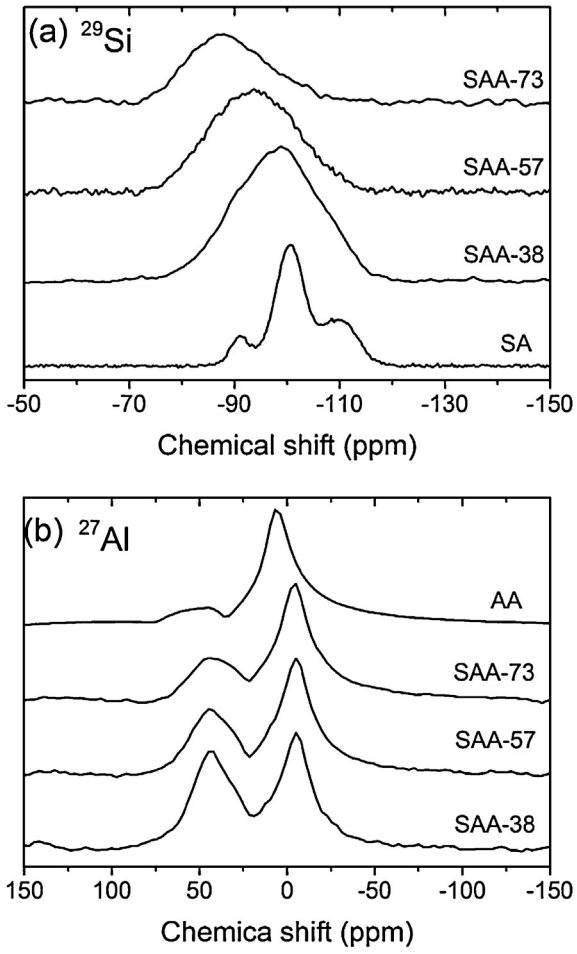

Fig. 3. Solid-state magic-angle spinning (MAS) (a) ^{29}Si and (b) ^{27}Al NMR spectra of SA, SAA-38, SAA-57, SAA-73, and AA.

of the peak areas, (Al(IV))/(Al(VI)), decreased with an increase in the Si content, yielding values of 0.12 (AA), 0.43 (SAA-73), 0.59 (SAA-57), and 1.03 (SAA-38) and exhibiting the possible formation of tetrahedral Al symmetry by Si substitution. Based on the observation that Al(IV) is responsible for the formation of strong Brönsted acid sites [75–82], the increasing ratio of Al(IV)/Al(VI) with an increase in Al/(Si + Al) indicates that more Brönsted acid sites form on SAA-38 and SAA-57 resulting in high catalytic activity, which corresponds to the observations by pyridine-FT-IR.

3.3. Conversion of benzyl phenyl ether mixed with acid-inhibiting 2,6-di-tert-butylpyridine

The BPE conversion on the Brönsted acid sites was confirmed by control experiments using a catalyst whose Brönsted acid sites were selectively blocked by the sterically hindered organic base of 2,6-di-*tert*-butylpyridine (2,6-DTBP) (Table 5 and Fig. S4) [83,84]. When 2,6-DTBP was introduced into the reaction system, the BPE conversion decreased drastically despite the fact that only a 2/1000 equivalent of 2,6-DTBP (0.18 μmol) of total acid sites (92.8 μmol on 0.1 g based on the NH_3-TPD result) was added. Good linearity between the BPE conversion and the 2,6-DTBP concentration was observed when amounts of 0.18, 0.45, and 0.89 μmol of 2,6-DTBP were added to each reactant (Fig. S4). These results demonstrate that BPE conversion must occur on the Brönsted acid sites.

3.4. Isomerization of benzyl phenyl ether on the precious-metal-free aerogel catalysts

The investigation of the BPE conversion results at 100–250 °C and the active sites for the isomerization process suggest a possible reaction pathway, as summarized in Fig. 4. The cracking of BPE during high temperature pyrolysis at 275–450 °C was suggested to occur with homolytic scission consisting of bond fission, hydrogen abstraction, and β-scission followed by radical termination steps [14,44,47,52–54], but the low temperature reaction (<250 °C) observed in this study may occur not via radical reactions but by different pathways. Instead of the phenoxy and benzyl radical intermediates suggested to occur during the pyrolysis of BPE [44,46,52,59,85], the carbocation intermediates on the acid catalysts can be included in the low temperature catalytic reaction pathway [58,60,86].

The Brönsted acid sites attracted ethers leading to a catalytic rearrangement to produce 2BP and 4BP possibly by Claisen rearrangement [87], which can be catalytically initiated at a temperature as low as room temperature [58,60]. The formation of 2BP was a primary reaction over that of 4BP regardless of the BPE conversion as reported in the literature (Fig. S5) [43,61,64]. Among the products, an appreciable amount of phenol was also obtained by the ether cleavage of BPE, but the formation of toluene was negligible as reported when acid catalysts were used [45]. Although the formation of toluene and phenol has been reported with sufficient hydrogen sources [44,88], 2BP and 4BP selectively formed under the H_2-deficient environment caused by the poor H_2-adsorbing SAA catalysts adopted in this study [61,64,89]. A GC/MS analysis of the product mixture indicated that trimers and dimers, including benzyltoluene, dibenzylphenol, and diphenylethane, were obtained by the combination of two toluenes (for the dimers including benzyltoluene and diphenylethane), and one phenol and two toluenes (for the trimers including dibenzylphenol), respectively. These observations indicate that the adsorbed toluene obtained by the ether cleavage of BPE may be quickly added to adjacent intermediates to form dimers and trimers as described in Fig. 4 [43]. The addition of cleaved fragments, particularly toluene, to the other fragments may be accelerated with the increasing reaction temperature, which suppressed the formation of 2BP and improved the formation of the trimer.

Table 5
Effects of 2,6-di-*tert*-butylpyridine (2,6-DTBP) on benzyl phenyl ether (BPE) conversion using SAA-38 (0.1 g) at 100 °C and 5 bar H_2.

Amount of 2,6-DTBP (μmol)	BPE conversion (mol%)	Yield (mol%)		
		Phenol	2BP	4BP
0.18	6.42	0	1.60	0
0.45	5.31	0	1.53	0
0.89	3.46	0	2.00	0
2.50	1.85	0	1.57	0
26.7	1.45	0	0	0

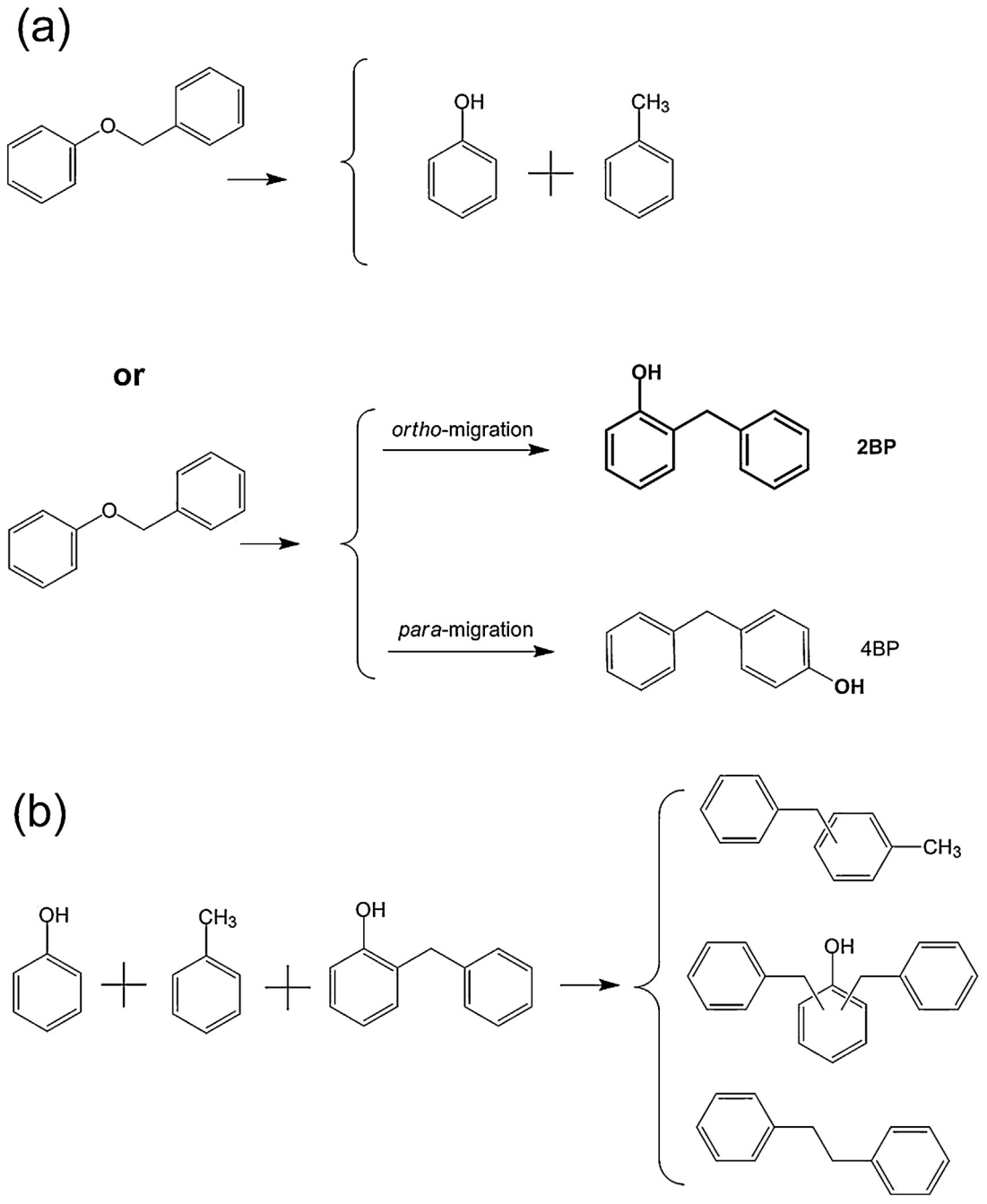

Fig. 4. Reaction pathway of benzyl phenyl ether conversion. (a) Formation of 2BP and 4BP. (b) Formation of dimers and trimers.

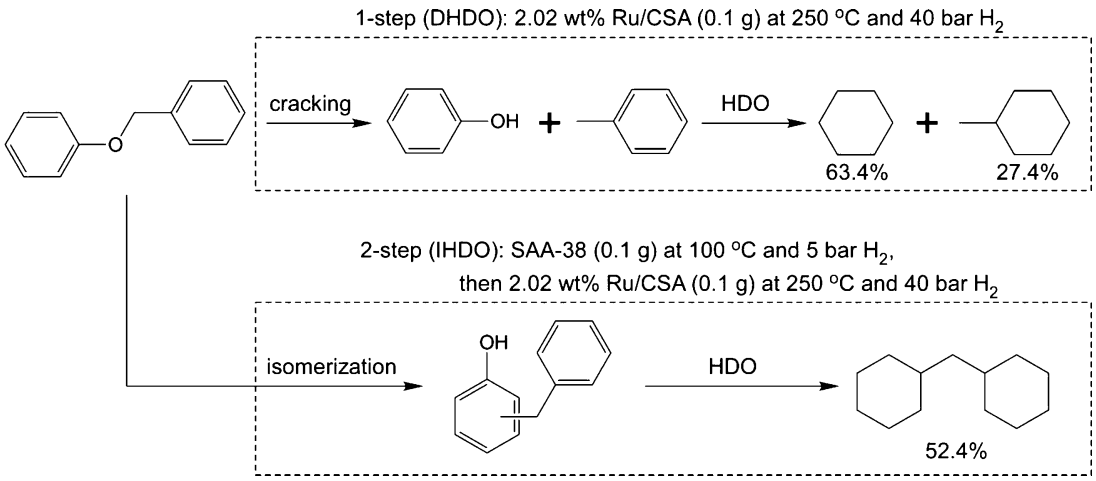

Fig. 5. Reaction schemes of (a) 1-step and (b) 2-step HDO of BPE.

Table 6
Hydrodeoxygenation (HDO) results of benzyl phenyl ether (BPE).

	Selectivity (%)[a]		
	Process I[b]	Process II[c]	Process III[d]
Methylcyclopentane (C6)	0.6	0.0	0.4
Cyclohexane (C6)	63.4	13.4	42.3
Methylcyclohexane (C7)	27.4	1.5	37.4
Cycloheptane (C7)	4.9	0.0	8.7
Dicyclohexylmethane (C13)	1.3	52.4	1.7
Sum of above products (%)	97.6	67.3	90.5

[a] Measured based on GC-FID peak area. All processes exhibited 100% BPE conversion.
[b] Process I: direct HDO (DHDO) using 2.02 wt% Ru/CSA (0.1 g) at 250 °C and 40 bar H_2 for 1 h.
[c] Process II: indirect HDO (IHDO) composed of the isomerization performed using SAA-38 (0.1 g) at 100 °C and 5 bar H_2 for 1 h, and then HDO performed using 2.02 wt% Ru/CSA (0.1 g) at 250 °C and 40 bar H_2 for 1 h.
[d] Process III: direct HDO (DHDO) using a physical mixture of 2.02 wt% Ru/CSA (0.1 g) and SAA-38 (0.1 g) at 250 °C and 40 bar H_2 for 1 h.

3.5. Two-step hydrodeoxygenation of benzyl phenyl ether using a bifunctional catalyst containing precious metal nanoparticles and solid acids

Based on the conversion of BPE to the phenolic dimers of 2BP and 4BP rather than the monomers of phenol and toluene on the solid acid aerogel catalysts, we designed a two-step reaction, or indirect HDO (IHDO), consisting of the isomerization of BPE to BPs on a silica-alumina catalyst and then the HDO of BPs on a supported noble metal catalyst (Fig. 5), which produces high carbon number dicyclohexyl hydrocarbons rather than monocyclohexyl compounds (Process II in Table 6). The first step of the IHDO of BPE was performed using SAA-38 at 100 °C and 5 bar H_2, producing a mixture of 2BP, 4BP, and phenol with 100% BPE conversion (Fig. 1). The second step of the IHDO process using the entire products of the first step was performed using 2.02 wt% Ru/CSA at 250 °C and 40 bar H_2, which finally produced predominant dicyclohexylmethane (C13 compound, 52.4% selectivity), cyclohexane (13.4% selectivity), methylcyclohexane (1.5% selectivity), and trimers (unidentified C19 compounds). In contrast to the IHDO, a one-step reaction, or direct HDO (DHDO), was performed using 2.02 wt% Ru/CSA at 250 °C and 40 bar H_2, which produced a large number of the C6-7 compounds (96.3% selectivity) of hydrogenated phenolic monomers [29] and a small number of the C13 compound of dicyclohexylmethane (1.3%) (Process I in Table 6). The stark difference between the one-step DHDO and the two-step IHDO processes can be attributed to the isomerization of BPE to BPs in IHDO, as performed on the noble-metal-free solid acid catalysts. To clarify the usefulness of IHDO, we also performed DHDO using a 1:1 (w/w) physical mixture of 2.02 wt% Ru/CSA and SAA-38 at 250 °C and 40 bar H_2 (process III in Table 6), which produced a tiny amount of dicyclohexylmehtane (1.7% selectivity) and a large amount of hydrogenated phenolic monomers or their derivatives including cyclohexane (42.3% selectivity), methylcyclohexane (37.4% selectivity), cycloheptane (8.7% selectivity), and methylcyclopentane (0.4% selectivity). These observations indicate that the two-step IHDO process selectively produces cyclic hydrocarbons with a higher carbon number compared to the one-step DHDO process, which produces the hydrocarbons with a smaller carbon number. In addition, five major compounds account for 90.5 and 97.6% of the products from the DHDO process but only 67.3% of the products from the IHDO process, as described in Table 6. The other products are mostly compounds with a higher carbon numbers, including hydrogenated phenolic trimers, thus indicating that the IHDO process (process II in Table 6) leads to the preferred production of high carbon number hydrocarbons. The formation of these hydrocarbons with a higher carbon number will be useful to those seeking to produce high-energy diesel fuels from lignin or lignin-derived fragments.

4. Conclusions

The conversion of BPE on acid catalysts of silica-alumina aerogels was observed to study the conversion of lignin or lignin-derivatives. BPE was converted to 4BP and 2BP by intramolecular rearrangement and phenol by the cleavage of ether bonds. The predominant formation of 2BP was attributed to Claisen-rearrangement. The characterizations including NH_3-TPD, NMR, and FT-IR, as well as a carefully designed control experiment indicated that catalytic activity was improved by the Brönsted acid sites. Based on the observed non-cracking isomerization of BPE, a two-step HDO was designed to produce high carbon number hydrocarbons. Deoxygenated C13–19 hydrocarbons rather than cracked C6–7 hydrocarbons were successfully obtained. According to these results, the two-step HDO process may be an efficient process to produce high carbon number hydrocarbons as possible alternative sources for diesel and jet fuel.

Acknowledgements

The authors thank Professor Jungkyu Choi (Korea University) for his valuable insight into the solid-acid characterization and catalysis data analysis. The authors also thank Dr. Doug Young

Han (Korea Basic Science Institute) the data collection for the ^{27}Al- and ^{29}Si-NMR. This work was supported by the National Research Foundation of Korea (NRF) grant funded by the Korean Government (MSIFP) (NRF-2009-C1AAA001-0093293), and by the 'Creative Allied Project (CAP)' grant funded by the Korea Research Concil of Fundamental Science and Technology (KRCF) and the Korea Institute of Science and Technology (KIST)

Appendix A. Supplementary data

Supplementary data associated with this article can be found, in the online version, at http://dx.doi.org/10.1016/j.apcatb.2013.05.039.

References

[1] R. Luque, L. Herrero-Davila, J.M. Campelo, J.H. Clark, J.M. Hidalgo, D. Luna, J.M. Marinas, A.A. Romero, Energy and Environmental Science 1 (2008) 542–564.
[2] P. Friedlingstein, I.C. Prentice, Current Opinion in Environmental Sustainability 2 (2010) 251–257.
[3] T.V. Choudhary, C.B. Phillips, Applied Catalysis A 397 (2011) 1–12.
[4] A. Demirbas, Applied Energy 88 (2011) 17–28.
[5] M. Fatih Demirbas, Applied Energy 86 (2009) S151–S161.
[6] F.W. Bai, W.A. Anderson, M. Moo-Young, Biotechnology Advances 26 (2008) 89–105.
[7] G. Anitescu, T.J. Bruno, Energy Fuels 26 (2012) 324–348.
[8] G.W. Huber, S. Iborra, A. Corma, Chemical Reviews 106 (2006) 4044–4098.
[9] M. Stöcker, Angewandte Chemie International Edition 47 (2008) 9200–9211.
[10] E. Adler, Wood Science and Technology 11 (1977) 169–218.
[11] J. Zakzeski, P.C.A. Bruijnincx, A.L. Jongerius, B.M. Weckhuysen, Chemical Reviews 110 (2010) 3552–3599.
[12] D.S.A.G. Radlein, J. Piskorz, D.S. Scott, Journal of Analytical and Applied Pyrolysis 12 (1987) 51–59.
[13] M. Kosa, H. Ben, H. Theliander, A.J. Ragauskas, Green Chemistry 13 (2011) 3196–3202.
[14] J. Akhtar, N.A.S. Amin, Renewable & Sustainable Energy Reviews 15 (2011) 1615–1624.
[15] L. Zhang, P. Champagne, C. Xu, Bioresource Technology 102 (2011) 8279–8287.
[16] J. Barbier, N. Charon, N. Dupassieux, A. Loppinet-Serani, L. Mahé, J. Ponthus, M. Courtiade, A. Ducrozet, A.-A. Quoineaud, F. Cansell, Biomass and Bioenergy 46 (2012) 479–491.
[17] Y. Ye, Y. Zhang, J. Fan, J. Chang, Industrial and Engineering Chemistry Research 51 (2012) 103–110.
[18] V.M. Roberts, V. Stein, T. Reiner, A. Lemonidou, X. Li, J.A. Lercher, Chemistry-A European Journal 17 (2011) 5939–5948.
[19] S. Son, F.D. Toste, Angewandte Chemie International Edition 49 (2010) 3791–3794.
[20] T.P. Vispute, H. Zhang, A. Sanna, R. Xiao, G.W. Huber, Science 330 (2010) 1222–1227.
[21] C. Zhao, J.A. Lercher, ChemCatChem 4 (2012) 64–68.
[22] A.G. Sergeev, J.F. Hartwig, Science 332 (2011) 439–443.
[23] C. Zhao, J.A. Lercher, Angewandte Chemie 124 (2012) 6037–6042.
[24] T. Nimmanwudipong, R. Runnebaum, S. Ebeler, D. Block, B. Gates, Catalysis Letters 142 (2012) 151–160.
[25] A.J. Foster, J. Jae, Y.-T. Cheng, G.W. Huber, R.F. Lobo, Applied Catalysis A 423–424 (2012) 154–161.
[26] X. Zhu, L.L. Lobban, R.G. Mallinson, D.E. Resasco, Journal of Catalysis 281 (2011) 21–29.
[27] A.L. Jongerius, R. Jastrzebski, P.C.A. Bruijnincx, B.M. Weckhuysen, Journal of Catalysis 285 (2012) 315–323.
[28] T. Nimmanwudipong, R. Runnebaum, D. Block, B. Gates, Catalysis Letters 141 (2011) 779–783.
[29] C.R. Lee, J.S. Yoon, Y.-W. Suh, J.-W. Choi, J.-M. Ha, D.J. Suh, Y.-K. Park, Catalysis Communications 17 (2012) 54–58.
[30] N. Yan, Y. Yuan, R. Dykeman, Y. Kou, P.J. Dyson, Angewandte Chemie International Edition 49 (2010) 5549–5553.
[31] S.K. Hanson, R. Wu, L.A.P. Silks, Angewandte Chemie 124 (2012) 3466–3469.
[32] V.N. Bui, D. Laurenti, P. Afanasiev, C. Geantet, Applied Catalysis B 101 (2011) 239–245.
[33] R. Runnebaum, T. Nimmanwudipong, R. Limbo, D. Block, B. Gates, Catalysis Letters 142 (2012) 7–15.
[34] J. He, C. Zhao, J.A. Lercher, Journal of American Chemical Society 134 (2012) 20768–20775.
[35] H.W. Park, S. Park, D.R. Park, J.H. Choi, I.K. Song, Korean Journal of Chemical Engineering 28 (2011) 1177–1180.
[36] N. Yan, C. Zhao, P.J. Dyson, C. Wang, L.-t. Liu, Y. Kou, ChemSusChem 1 (2008) 626–629.
[37] D.J. Suh, T.-J. Park, J.H. Sonn, J.-C. Lim, Journal of Materials Science Letters 18 (1999) 1473–1475.
[38] D.J. Suh, Journal of Non-Crystalline Solids 350 (2004) 314–319.
[39] E.P. Barrett, L.G. Joyner, P.P. Halenda, Journal of American Chemical Society 73 (1951) 373–380.
[40] D.J. Suh, T.-J. Park, Journal of Materials Science Letters 16 (1997) 490–492.
[41] D.J. Suh, T.-J. Park, Chemistry of Materials 8 (1996) 509–513.
[42] C.A. Emeis, Journal of Catalysis 141 (1993) 347–354.
[43] M.H. Bhure, C.V. Rode, R.C. Chikate, N. Patwardhan, S. Patil, Catalysis Communications 8 (2007) 139–144.
[44] R.H. Schlosberg, J. William, H. Davis, T.R. Ashet, Fuel 60 (1981) 201–204.
[45] H. Matsuhashi, H. Hattori, K. Tanabe, Fuel 64 (1985) 1224–1228.
[46] Y. Sato, T. Yamakawa, Industrial and Engineering Chemistry Research Fundamentals 24 (1985) 12–15.
[47] B.C. Wu, M.T. Klein, S.I. Sandler, Energy Fuels 5 (1991) 453–458.
[48] R. Malhotra, D.F. McMillen, Energy Fuels 7 (1993) 227–233.
[49] A.R. Katritzky, S.M. Allin, M. Siskin, Accounts of Chemical Research 29 (1996) 399–406.
[50] K. Shimizu, K. Miki, I. Saitou, Fuel 76 (1997) 23–27.
[51] A.C. Buchanan, P.F. Britt, J.T. Skeen, J.A. Struss, C.L. Elam, Journal of Organic Chemistry 63 (1998) 9895–9903.
[52] E. Dorrestijin, L.J.J. Laarhoven, I.W.C.E. Arends, P. Mulder, Journal of Analytical and Applied Pyrolysis 54 (2000) 153–192.
[53] M.K. Kidder, P.F. Britt, I.A.C. Buchanan, Energy Fuels 20 (2006) 54–60.
[54] D.F. McMillen, R. Malhotra, The Journal of Physical Chemistry A 110 (2006) 6757–6770.
[55] V. Roberts, S. Fendt, A.A. Lemonidou, X. Li, J.A. Lercher, Applied Catalysis B 95 (2010) 71–77.
[56] X.Y. Wu, X.Y. Lü, Chinese Chemical Letters 22 (2011) 733–737.
[57] M.B. Smith, J. March, March's advanced organic chemistry: reactions, mechanisms, and structure, 6th ed., John Wiley & Sons, Hoboken, New Jersey, USA, 2007.
[58] A.M. Martín Castro, Chemical Reviews 104 (2004) 2939–3002.
[59] B.C. Wu, M.T. Klein, S.I. Sandler, AIChE Journal 36 (1990) 1129–1136.
[60] R.P. Lutz, Chemical Reviews 84 (1984) 205–247.
[61] D.S. Tarbell, J.C. Petropoulos, Journal of American Chemical Society 74 (1952) 244–248.
[62] D.S. Tarbell, Chemical Reviews 27 (1940) 495–546.
[63] D.J. Suh, T.-J. Park, H.-Y. Han, J.-C. Lim, Chemistry of Materials 14 (2002) 1452–1454.
[64] L.S. Hart, C.R. Waddington, Journal of the Chemical Society, Perkin Transactions 2 (1985) 1607–1612.
[65] R. Anand, R. Maheswari, U. Hanefeld, Journal of Catalysis 242 (2006) 82–91.
[66] F. Lónyi, J. Valyon, Thermochimica Acta 373 (2001) 53–57.
[67] R. Barthos, F. Lónyi, G. Onyestyák, J. Valyon, Journal of Physical Chemistry B 104 (2000) 7311–7319.
[68] C.V. Hidalgo, H. Itoh, T. Hattori, M. Niwa, Y. Murakami, Journal of Catalysis 85 (1984) 362–369.
[69] N.Y. Topsøe, K. Pedersen, E.G. Derouane, Journal of Catalysis 70 (1981) 41–52.
[70] H.G. Karge, Comparative Measurements on Acidity of Zeolites (1991) 133–156.
[71] F. Hao, J. Zhong, P.-L. Liu, K.-Y. You, H.-A. Luo, Journal of Molecular Catalysis A: Chemical 363–364 (2012) 41–48.
[72] W.-H. Chen, H.-H. Ko, A. Sakthivel, S.-J. Huang, S.-H. Liu, A.-Y. Lo, T.-C. Tsai, S.-B. Liu, Catalysis Today 116 (2006) 111–120.
[73] G. Crépeau, V. Montouillout, A. Vimont, L. Mariey, T. Cseri, F. Maugé, Journal of Physical Chemistry B 110 (2006) 15172–15185.
[74] G. Engelhardt, D. Michel, High-resolution solid-statre NMR of silicates and zeolites, John Wiley & Sons, Chichester, UK, 1987.
[75] B. Xu, C. Sievers, J.A. Lercher, J.A.R. van Veen, P. Giltay, R. Prins, J.A. van Bokhoven, Journal of Physical Chemistry C 111 (2007) 12075–12079.
[76] D.R. Milburn, R.A. Keogh, R. Srinivasan, B.H. Davis, Applied Catalysis A 147 (1996) 109–125.
[77] A. Corma, Current Opinion in Solid State and Materials Science 2 (1997) 63–75.
[78] Z. Yu, S. Li, Q. Wang, A. Zheng, X. Jun, L. Chen, F. Deng, Journal of Physical Chemistry C 115 (2011) 22320–22327.
[79] A. Omegna, J.A. van Bokhoven, R. Prins, Journal of Physical Chemistry B 107 (2003) 8854–8860.
[80] J.A. van Bokhoven, A.L. Roest, D.C. Koningsberger, J.T. Miller, G.H. Nachtegaal, A.P.M. Kentgens, Journal of Physical Chemistry B 104 (2000) 6743–6754.
[81] A.A. Gurinov, Y.A. Rozhkova, A. Zukal, J.i. Cejka, I.G. Shenderovich, Langmuir 27 (2011) 12115–12123.
[82] M. Selvaraj, A. Pandurangan, P.K. Sinha, Industrial and Engineering Chemistry Research 43 (2004) 2399–2412.
[83] C.D. Baertsch, K.T. Komala, Y.-H. Chua, E. Iglesia, Journal of Catalysis 205 (2002) 44–57.
[84] R. Gounder, A.J. Jones, R.T. Carr, E. Iglesia, Journal of Catalysis 286 (2012) 214–223.
[85] P.F. Britt, A.C. Buchanan, K.B. Thomas, S.-K. Lee, Journal of Analytical and Applied Pyrolysis 33 (1995) 1–19.
[86] M.J.S. Dewar, P.A. Spanninger, Journal of the Chemical Society, Perkin Transactions 2 (1972) 1204–1206.
[87] S. Ozawa, T. Suenaga, Y. Ogino, Fuel 64 (1985) 712–714.
[88] R.H. Schlosberg, T.R. Ashe, R.J. Pancirov, M. Donaldson, Fuel 60 (1981) 155–157.
[89] A.C. Buchanan, P.F. Britt, K.B. Thomas, C.A. Biggs, Energy Fuels 7 (1993) 373–379.